

Propagation dynamics of a temporally, amplitude- and group-velocity-matched two-mode ultraslow wave in a three-level Λ system

L. Deng, M. G. Payne, and E. W. Hagley

Electron and Optics Physics Division, NIST, Gaithersburg, Maryland 20899, USA

(Received 25 August 2003; revised manuscript received 19 March 2004; published 22 December 2004)

We investigate the propagation dynamics of a two-mode probe field traveling with ultraslow group velocities. We show that a strong cross-beam coupling occurs between the two modes of the probe wave in the presence of a two-mode control laser field that maintains two-photon resonance excitations in a three-level Λ system. In the adiabatic limit and under appropriate conditions, both modes can travel with matched temporal profiles, amplitudes, and greatly reduced group velocities, and one mode can grow and take on features of the other mode. When only one mode of probe field is injected, the generation and growth of the second mode has the characteristics of four-wave mixing, resulting in a tunable, ultraslow four-wave mixing field with nearly 100% photon flux conversion efficiency. We further show a type of induced transparency resulting from an efficient one- and three-photon destructive interference. This is to be contrasted with the conventional one-mode, three-level electromagnetically induced transparency where the interference involves two one-photon pathways.

DOI: 10.1103/PhysRevA.70.063813

PACS number(s): 42.50.Gy, 42.65.-k, 42.25.Bs

I. INTRODUCTION

Ultraslow propagation of optical waves in highly resonant and ultracold media under electromagnetically induced transparency (EIT) [1] conditions has been considered as one of the promising candidates for quantum information manipulation [2]. This has motivated several recent studies that have demonstrated ultraslow propagation [3]. In addition, some very efficient nonlinear processes using EIT techniques have also been proposed [4–14]. Despite this progress, a systematic treatment and understanding of group-velocity-matched ultraslow propagation of multiple fields using a single-specie three-level medium is not available in the literature. Here we investigate the propagation dynamics of a two-mode [15] ultraslow wave in a single-specie three-state Λ system [16]. We show that in this two-mode configuration a strong cross-beam coupling between the two weak probe beams occurs. In the adiabatic limit, each probe pulse breaks up into two pulses that propagate at different group velocities. With appropriately chosen parameters, however, this pulse breakup can be eliminated, resulting in a two-mode temporally, amplitude, and group velocity (TAG) matched ultraslow probe wave in a single-specie three-level medium [17]. In addition, we show that at a suitable propagation distance, where the components of the fast decaying waves in both modes have become negligible, an effective multiphoton destructive interference occurs [18], resulting in an interference which leads to a new type of highly efficient induced transparency. We further extend our treatment to the case of two temporally delayed input probe pulses of different frequencies and show that group-velocity-matchable propagation of such a delayed pulse pair can also be achieved in the same single-specie three-level medium. The realization of such a TAG-matched ultraslow pulse pair in a single-specie three-level medium may have important applications in high-fidelity quantum information storage, photon pair entanglement, and quantum computing. When only a single-frequency probe

field is injected into the medium, we show that the two-mode configuration has the characteristics of a four-wave mixing (FWM) process and can achieve near unity photon flux conversion efficiency from one mode to the other [19] without the requirement of having maximum atomic coherence [4]. Thus, by adjusting one of the two one-photon detunings, one can obtain a highly efficient yet tunable coherent source.

II. FOUR-WAVE MIXING IN A Λ SYSTEM

We consider a lifetime-broadened three-level Λ system as depicted in Fig. 1. A two-mode, pulsed (pulse length τ at the entrance of the medium) probe field and a two-mode continuous wave (cw) control field complete the respective exact two-photon resonance excitations between states $|1\rangle$ and $|3\rangle$. Let us assume that the probe lasers are weak so that almost all of the population remains in $|1\rangle$. Using this assumption and neglecting cross-mode-stimulated emission, we obtain the equations of motion for the atomic response and probe fields:

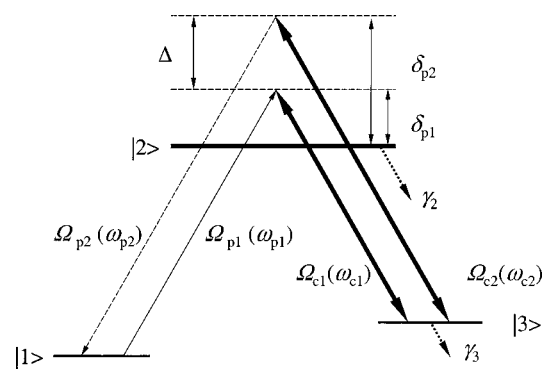


FIG. 1. Energy-level diagram for a three-state system interacting with a two-mode probe field and a two-mode control field. δ_{p1} and δ_{p2} are the two one-photon detunings, Ω_{pn} and Ω_{cn} ($n=1,2$) are half of the Rabi frequencies for the probe and control fields.

$$\left(\frac{\partial A_2^{(1)}}{\partial(t_r/\tau)}\right)_z = id_{p1}\tau A_2^{(1)} + i\Omega_{c1}^*\tau A_3 + i\Omega_{p1}^*\tau, \quad (1a)$$

$$\left(\frac{\partial A_2^{(2)}}{\partial(t_r/\tau)}\right)_z = id_{p2}\tau A_2^{(2)} + i\Omega_{c2}^*\tau A_3 + i\Omega_{p2}^*\tau, \quad (1b)$$

$$\left(\frac{\partial A_3}{\partial(t_r/\tau)}\right)_z = id_3\tau A_3 + i\Omega_{c1}\tau A_2^{(1)} + i\Omega_{c2}\tau A_2^{(2)}, \quad (1c)$$

$$\left(\frac{\partial \Omega_{pn}^*\tau}{\partial z}\right)_{t_r/\tau} = i\kappa_{12}\tau A_2^{(n)} \quad (n=1,2). \quad (1d)$$

Here $A_2^{(n)}$ ($n=1,2$) is the part of state $|2\rangle$'s amplitude that carries the polarization at angular frequency ω_{pn} , $d_{pn} = \delta_{pn} + i\gamma_2/2$, δ_{pn} is the detuning of the ω_{pn} mode probe laser from the $|1\rangle \rightarrow |2\rangle$ resonance, and γ_2 is the decay rate of state $|2\rangle$. In addition, A_3 is the amplitude of state $|3\rangle$, $d_3 = \delta_3 + i\gamma_3/2$, with $\delta_3 = \omega_{p1} - \omega_{c1} = \omega_{p2} - \omega_{c2}$ being a two-photon detuning between states $|1\rangle$ and $|3\rangle$ and γ_3 being the decay rate of state $|3\rangle$ [20]. In the following calculation we will assume that the two-photon resonances are always maintained so that $\delta_3 = 0$. Finally, Ω_{pn} and Ω_{cn} are the half-Rabi frequencies of the probe and control fields for the relevant frequency mode and $k_{12} = 2\pi N\omega_{pn}|D_{12}|^2/(\hbar c)$, with N and D_{12} being the concentration and the dipole moment for the transition $|1\rangle \rightarrow |2\rangle$, respectively. In deriving Eqs. (1a)–(1d) we have taken $A_1 \simeq 1$, defined $t_r = t - z/c$, and also made the necessary phase transformation to remove all of the complex phase factors.

The steps for solving Eqs. (1a)–(1d) begin with assumptions that $|d_{pn}\tau| \gg 1$, $|\delta_{p2}| \gg |\Omega_{pn}|$ ($n=1,2$), $\sum_{n=1}^2 |\Omega_{cn}\tau|^2 / |\delta_{pn}\tau| \gg 1$, and $|\Omega_{pn}| \ll |\Omega_{cn}|$. These conditions ensure that the ground state is undepleted and the adiabatic processes remain effective. The latter requirement is the key for possible analytical solutions to Eqs. (1a)–(1d). Let $\alpha_2^{(n)}$ and α_3 be the time Fourier transforms of $A_2^{(n)}$ and A_3 , η be the dimensionless time Fourier transform variable, and Λ_{pn}^* be the time Fourier transforms of Ω_{pn}^* , respectively. We obtain

$$\alpha_2^{(1)} = \frac{[|\Omega_{c2}\tau|^2 - (d_3\tau + \eta)(d_{p2}\tau + \eta)]\Lambda_{p1}^*\tau - \Omega_{c1}^*\tau\Omega_{c2}\tau\Lambda_{p2}^*\tau}{D}, \quad (2a)$$

$$\alpha_2^{(2)} = \frac{[|\Omega_{c1}\tau|^2 - (d_3\tau + \eta)(d_{p1}\tau + \eta)]\Lambda_{p2}^*\tau - \Omega_{c2}^*\tau\Omega_{c1}\tau\Lambda_{p1}^*\tau}{D}, \quad (2b)$$

$$\alpha_3 = -\frac{\Omega_{c1}\tau(d_{p2}\tau + \eta)\Lambda_{p1}^*\tau + \Omega_{c2}\tau(d_{p1}\tau + \eta)\Lambda_{p2}^*\tau}{D}, \quad (2c)$$

$$\frac{\partial \Lambda_{pn}\tau}{\partial z} = i\kappa_{12}\tau\alpha_2^{(n)} \quad (n=1,2), \quad (2d)$$

where $D = (d_{p1}\tau + \eta)(d_{p2}\tau + \eta)(d_3\tau + \eta) - |\Omega_{c1}\tau|^2(d_{p2}\tau + \eta) - |\Omega_{c2}\tau|^2(d_{p1}\tau + \eta)$. Equations (2a)–(2d) can be easily solved, yielding

$$\Lambda_{pn}^* = e^{\alpha_p z}(W_+^{(n)} + e^{Lz} + W_-^{(n)}e^{-Lz}) \quad (n=1,2), \quad (3)$$

where we have defined the quantities

$$\alpha_p = \frac{L_0}{2} \sum_{n=1}^2 [|\Omega_{cn}\tau|^2 - (d_3\tau + \eta)(d_{pn}\tau + \eta)],$$

$$L_0 = \frac{i\kappa_{12}\tau}{(d_{p1}\tau + \eta)(d_{p2}\tau + \eta)(d_3\tau + \eta) - J},$$

$$J = (d_{p1}\tau + \eta)|\Omega_{c2}\tau|^2 + (d_{p2}\tau + \eta)|\Omega_{c1}\tau|^2,$$

$$W_{\pm}^{(1)} = \frac{(L \pm \alpha_m)\Lambda_{p1}^*(0, \eta)\tau \pm \alpha_{12}\Lambda_{p2}^*(0, \eta)\tau}{2L},$$

$$L = L_0\sqrt{\beta_m^2 + \beta_{12}^2}, \quad \alpha_m = L_0\beta_m,$$

$$\beta_m = \frac{|\Omega_{c1}\tau|^2 - |\Omega_{c2}\tau|^2 - (d_{p1}\tau - d_{p2}\tau)(d_3\tau + \eta)}{2},$$

$$\alpha_{12} = -L_0\beta_{12}, \quad \beta_{12} = \Omega_{c1}^*\tau\Omega_{c2}\tau,$$

$$W_{\pm}^{(2)} = \frac{(L \pm \alpha_m)\Lambda_{p2}^*(0, \eta)\tau \pm \alpha_{21}\Lambda_{p1}^*(0, \eta)\tau}{2L}.$$

The remaining step is to take the inverse Fourier transform of Eq. (3) using the above-defined quantities so that physical insight can be gained. In general, this is difficult because of the complex expressions of these quantities. In the following we will first examine regimes that are important to highly efficient wave-mixing processes, yet also allow insightful analytical solutions of the field equations. Later, we compare these analytical solutions with a full numerical inverse transform of Eq. (3) to establish the validity of the analytical solutions in the regimes under study. We will show that the analytical solutions obtained agree well with numerical solutions under the conditions specified. We note that the major approximations in obtaining these analytical solutions are the undepleted ground state and the neglecting of far-off-resonant terms such as cross-mode-stimulated emission with nonvanishing two-photon detunings (these approximations should always be accurate if the fields at ω_{p1} and ω_{p2} are sufficiently weak). Beyond these no other approximations have been made in our semi classical theory.

III. APPROXIMATE ANALYTICAL SOLUTIONS TO THE FIELD EQUATIONS

Although in general detailed solutions of the field equations require numerical evaluation of Eq. (3) using the complex quantities defined thereafter, much physical insight can be gained if the exponents—i.e., $\alpha_p \pm L$ —can be approximated as linear or quadratic functions of η . The linear dependence on η will correctly predict the propagation velocities of the two probe fields, whereas the inclusion of the quadratic terms in η provides corrections to both the field amplitude and group velocity due to pulse spreading and

additional pulse attenuation. We note that the quadratic approximation can be quite accurate even when $\gamma_2\tau$ is relatively large, as with the lowest $S \rightarrow P$ transitions in alkali elements. Typically, when the linear or quadratic approximation to $\alpha_p \pm L$ is accurate, it is sufficiently accurate to simply evaluate the coefficients in the expression of $W_{\pm}^{(n)}$ evaluated at $\eta=0$. This is a consequence of the linear and quadratic terms being small corrections to a much larger constant term in these coefficients. With these approximations we have (defining $|\Omega\tau|^2 = |\Omega_{c1}\tau|^2 + |\Omega_{c2}\tau|^2$)

$$W_{+}^{(1)} = \frac{|\Omega_{c2}|^2}{|\Omega|^2} \left(\Lambda_{p1}^*(0, \eta) - \frac{\Omega_{c1}^*}{\Omega_{c2}^*} \Lambda_{p2}^*(0, \eta) \right), \quad (4a)$$

$$W_{-}^{(1)} = \frac{|\Omega_{c1}|^2}{|\Omega|^2} \left(\Lambda_{p1}^*(0, \eta) + \frac{\Omega_{c2}}{\Omega_{c1}} \Lambda_{p2}^*(0, \eta) \right), \quad (4b)$$

$$W_{+}^{(2)} = \frac{|\Omega_{c2}|^2}{|\Omega|^2} \left(\Lambda_{p2}^*(0, \eta) - \frac{\Omega_{c1}}{\Omega_{c2}} \Lambda_{p1}^*(0, \eta) \right), \quad (4c)$$

$$W_{-}^{(2)} = \frac{|\Omega_{c1}|^2}{|\Omega|^2} \left(\Lambda_{p2}^*(0, \eta) + \frac{\Omega_{c2}^*}{\Omega_{c1}^*} \Lambda_{p1}^*(0, \eta) \right). \quad (4d)$$

In arriving at Eqs. (4a)–(4d) we have assumed that $|\Omega_{cn}\tau|^2 \gg |(d_{pn}\tau + \eta)(d_3\tau + \eta)|$ (for $n=1, 2$) and $|J| \gg |(d_{p1}\tau + \eta)(d_{p2}\tau + \eta)(d_3\tau + \eta)|$.

We first consider the limit where adiabatic behavior of $A_2^{(n)}$ is expected to be a good first approximation and the assumption of nondepleted ground-state population is valid. This is the limit where the validity of Eqs. (4a)–(4d) and the assumptions leading to these equations are ensured. Under these assumptions the series expansion in η converges rapidly and excited-state amplitudes remain small. In this limit we use Eqs. (4a)–(4d) and retain only the constant and linear terms in η in the exponents of Eq. (3). This allows analytical evaluation of the inverse Fourier transform of Eq. (3). We thus obtain

$$\begin{aligned} \Omega_{p1}^* \left(z, \frac{t_r}{\tau} \right) = & r \frac{|\Omega_{c1}|^2}{|\Omega|^2} \left[\Omega_{p1}^* \left(0, t - \frac{z}{V_g^{(-)}} \right) + \frac{\Omega_{c2}}{\Omega_{c1}} \Omega_{p2}^* \left(0, t - \frac{z}{V_g^{(-)}} \right) \right] \\ & + \frac{|\Omega_{c2}|^2 e^{-i\kappa_{12}\tau\Omega\tau^2 z/J}}{|\Omega|^2} \left[\Omega_{p1}^* \left(0, t - \frac{z}{V_g^{(+)}} \right) - \frac{\Omega_{c1}^*}{\Omega_{c2}^*} \Omega_{p2}^* \left(0, t - \frac{z}{V_g^{(+)}} \right) \right], \end{aligned} \quad (5a)$$

$$\begin{aligned} \Omega_{p2}^* \left(z, \frac{t_r}{\tau} \right) = & r \frac{|\Omega_{c1}|^2}{|\Omega|^2} \left[\Omega_{p2}^* \left(0, t - \frac{z}{V_g^{(-)}} \right) + \frac{\Omega_{c2}^*}{\Omega_{c1}^*} \Omega_{p1}^* \left(0, t - \frac{z}{V_g^{(-)}} \right) \right] \\ & + \frac{|\Omega_{c2}|^2 e^{-i\kappa_{12}\tau\Omega\tau^2 z/J}}{|\Omega|^2} \left[\Omega_{p2}^* \left(0, t - \frac{z}{V_g^{(+)}} \right) - \frac{\Omega_{c1}}{\Omega_{c2}} \Omega_{p1}^* \left(0, t - \frac{z}{V_g^{(+)}} \right) \right], \end{aligned} \quad (5b)$$

where $V_g^{(\pm)}$ are given by

$$\frac{1}{V_g^{(+)}} = \frac{1}{c} + \frac{\kappa_{12}}{|\Omega|^2} \left[\frac{(d_{p1}\tau - d_{p2}\tau)^2 |\Omega_{c1}\tau|^2 |\Omega_{c2}\tau|^2}{J^2} \right], \quad (6a)$$

$$\frac{1}{V_g^{(-)}} = \frac{1}{c} + \frac{\kappa_{12}}{|\Omega|^2}, \quad (6b)$$

and $r = \exp[-\gamma_3 z / (2V_g^{(-)})]$. We note that it is the eigenvalue $\alpha_p - L$ that leads to the very slow decay as a function of propagation distance and also leads naturally to a group velocity that has the conventional EIT functional form—i.e., Eq. (6b).

Equations (5) and (6) indicate that each probe mode breaks up into two groups of pulses, each traveling at a different group velocity. One way to optimize the generated FWM field (i.e., the ω_{p2} mode) and obtain identical group velocities for the two components is to choose $|\Omega_{c1}| = |\Omega_{c2}|$ and $\delta_{p1} = 0$ together with $|\delta_{p2}| \gg \gamma_2/2$. With these choices, $J \approx \delta_{p2}\tau|\Omega\tau|^2/2$ and $(d_{p1}\tau - d_{p2}\tau)^2 |\Omega_{c1}|^2 |\Omega_{c2}|^2 \approx (\delta_{p2}\tau)^2 |\Omega\tau|^4/4 \approx J^2$. Thus, we have closely matched group velocities for the various pulse components:

$$\frac{1}{V_g^{(+)}} \approx \frac{1}{c} + \frac{\kappa_{12}}{|\Omega|^2} = \frac{1}{V_g^{(-)}}. \quad (7)$$

If we assume that initially there is no field in the ω_{p2} mode at the entrance to the medium [i.e., $\Omega_{p2}(0, t) = 0$], by maximizing the amplitude of the generated FWM field (ω_{p2} mode) and by maintaining group velocity matched, we have

$$\begin{aligned} \Omega_{p1}^* (z, t/\tau) = & \frac{1}{2} [r \Omega_{p1}^* (0, t - z/V_g^{(-)}) + e^{-i2\kappa_{12}\tau z / (\delta_{p2}\tau + i\gamma_2\tau)} \\ & \times \Omega_{p1}^* (0, t - z/V_g^{(-)})], \end{aligned} \quad (8a)$$

$$\begin{aligned} \Omega_{p2}^* (z, t/\tau) = & \frac{1}{2} [r \Omega_{p1}^* (0, t - z/V_g^{(-)}) - e^{-i2\kappa_{12}\tau z / (\delta_{p2}\tau + i\gamma_2\tau)} \\ & \times \Omega_{p1}^* (0, t - z/V_g^{(-)})]. \end{aligned} \quad (8b)$$

We note that if $\gamma_3\tau \ll 1$, as is the case when state $|3\rangle$ is a member of the ground-state manifold, then when $\exp(-2\kappa_{12}\gamma_2 z / \delta_2^2)$ is close to unity the amplitudes of the two terms in Eq. (8a) [and also in Eq. (8b)] are nearly the same. In this case, if $2\kappa_{12}z / \delta_2 = m\pi$ and m is an odd integer, we get $\Omega_{p1}^*(z, t) = 0$ and $\Omega_{p2}^*(z, t) = \Omega_{p1}^*(0, t - z/V_g^{(-)})$. Therefore, with an appropriate medium thickness, the field that exits the resonant medium will only be the FWM field (i.e., the ω_{p2} mode) with an amplitude nearly equal to that of the ω_{p1} mode probe field at the entrance of the medium. Since the frequencies of the two fields are nearly equal in the system discussed here, this represents a 100% conversion of the probe field (ω_{p1} mode) to a FWM field (ω_{p2} mode). On the other hand, if m is an even integer, the FWM field is zero and the amplitude of the ω_{p1} mode field is nearly the same as its initial value. Thus, as the two interacting fields propagate through the medium, the state of the probe field oscillates between the two field modes as a function of propagation distance. Note that in this problem there can be nearly 100% conversion efficiency, but there are certainly no conditions or restrictions on having maximum coherence. Indeed, there is

almost no ($\ll 1$) excited-state population in this problem. This is very different from other high-efficiency frequency converters based on a Raman double- Λ system [4].

We further note that both Ω_{p1}^* and Ω_{p2}^* [see Eqs. (5a) and (5b)] have a velocity component (i.e., the $V_g^{(+)}$ component) that decays in exactly the same way. In the case where only $\Omega_{p1}^*(0, t)$ is nonzero this feature has very interesting implications. From Eqs. (5a) and (5b) and at large z where the fast decaying part is negligible, we get a TAG ultraslow matched pulse pair (when $|\Omega_{c1}| = |\Omega_{c2}|$)

$$\Omega_{p1}^*(z, t/\tau) = r \frac{|\Omega_{c1}|^2}{|\Omega|^2} \Omega_{p1}^*(0, t - z/V_g^{(-)}), \quad (9a)$$

$$\Omega_{p2}^*(z, t/\tau) = r \frac{\Omega_{c1} \Omega_{c2}^*}{|\Omega|^2} \Omega_{p1}^*(0, t - z/V_g^{(-)}). \quad (9b)$$

This leads to

$$\frac{\Omega_{p1}^*(z, t/\tau)}{\Omega_{p2}^*(z, t/\tau)} = \frac{\Omega_{c1}^*}{\Omega_{c2}^*}. \quad (10)$$

The interesting consequence of this result is that $\Lambda_{p1}^* = (\Omega_{c1}^*/\Omega_{c2}^*)\Lambda_{p2}^*$. Using this result on the right-hand sides of Eqs. (2a) and (2b) and assuming $|\Omega_{cn}\tau|^2 \gg |\eta d_{pn}\tau|$ (for $n = 1, 2$), we immediately get

$$\alpha_2^{(1)} + \alpha_2^{(2)} = \frac{\eta(d_{p1}\tau + d_{p2}\tau\Omega_{c2}^*/\Omega_{c1}^*)\Lambda_{p1}^*\tau}{|\Omega_{c1}\tau|^2(d_{p2}\tau + \eta) + |\Omega_{c2}\tau|^2(d_{p1}\tau + \eta)} \approx 0.$$

This implies that at a sufficient depth into the medium where Eqs. (9a) and (9b) are valid the amplitude of A_2 is strongly suppressed by a destructive interference between a one- (Ω_{p1}^*) and three ($\Omega_{c1}^*, \Omega_{c2}^*, \Omega_{p2}^*$) photon pathways to drive the $|1\rangle \rightarrow |2\rangle$ transition. Consequently, a new type of induced transparency is established and the medium becomes highly transparent to the pair of ultraslow probe pulses. This type of destructive interference has been pointed out earlier in another highly efficient FWM process by Payne and Deng [13]. As a consequence of this three-photon destructive interference, if two matched pulses satisfying Eq. (10) are injected into the medium, they will propagate with identical temporal profiles, amplitudes, and group velocities and suffer very little distortion or attenuation.

The above results are the consequence of the linearization of the coefficients and exponents permitted by the assumption of good adiabatic behavior in the atomic response. Corrections to such a strict adiabatic theory of atomic response can be derived analytically to account for probe pulse spreading and additional attenuation. Such corrections due to higher-order nonadiabatic contributions play an important role when the control laser Rabi frequencies are significantly reduced, as required for achieving steep group velocity reduction in a conventional three-level Λ -type EIT operation. To include these corrections we take

$$\alpha_p + L = ib_0 + ib_1\eta + ib_2\eta^2, \quad (11a)$$

$$\alpha_p - L = ic_0 + ic_1\eta + ic_2\eta^2, \quad (11b)$$

where

$$b_0 = -\frac{\kappa_{12}\tau}{2J} |\Omega\tau|^2, \quad b_1 = -b_0 \frac{(d_{p1}\tau - d_{p2}\tau)^2 |\Omega_{c1}\tau|^2 |\Omega_{c2}\tau|^2}{|\Omega\tau|^4 J},$$

$$b_2 = -b_1 \frac{(d_{p1}\tau - d_{p2}\tau)(d_{p1}\tau |\Omega_{c2}\tau|^4 - d_{p2}\tau |\Omega_{c1}\tau|^4)}{|\Omega\tau|^4 J},$$

$$c_0 = \frac{\gamma_3\tau}{2} \frac{\kappa_{12}\tau}{|\Omega\tau|^2}, \quad c_1 = c_0 \frac{2}{\gamma_3\tau},$$

$$c_2 = c_1 \frac{d_{p1}\tau |\Omega_{c1}\tau|^2 + d_{p2}\tau |\Omega_{c2}\tau|^2}{|\Omega\tau|^4}.$$

Substituting Eqs. (11a) and (11b) into Eq. (3) and taking the inverse transform, one arrives at expressions for both modes of the probe field that properly include attenuation and pulse spreading under these conditions. To be more specific, we now consider two probe pulses with the initial shapes

$$\Omega_{p1}^*(0, t/\tau) = \Omega_{p1}^*(0, 0) e^{-2t^2/\tau^2}, \quad (12a)$$

$$\Omega_{p2}^*(0, t/\tau) = \Omega_{p2}^*(0, t_d/\tau) e^{-2(t - t_d)^2/(\tau f)^2}. \quad (12b)$$

In this case the two probe fields at the entrance of the medium ($z=0$) have different widths and amplitudes and may even peak at different times via a time-delay parameter t_d . The control over the width of the second probe field is through the parameter f . Following the procedure described above, we obtain the probe pulse in the ω_{p1} frequency mode:

$$\Omega_{p1}^*(z, t_r/\tau) = \Omega_{p1+}^*(z, t_r/\tau) + \Omega_{p1-}^*(z, t_r/\tau), \quad (13a)$$

where

$$\begin{aligned} \Omega_{p1+}^* &= \Omega_{p1}^*(0, 0) e^{ib_0 z} \frac{|\Omega_{c2}|^2}{|\Omega|^2 \sqrt{1 - 8ib_2 z}} \exp\left(-\frac{2(t_r/\tau - b_1 z)^2}{1 - 8ib_2 z}\right) \\ &\quad - \Omega_{p2}^*(0, t_d/\tau) e^{ib_0 z} \frac{\Omega_{c2}^* \Omega_{c1}}{|\Omega|^2 \sqrt{1 - 8ib_2 z/f^2}} \\ &\quad \times \exp\left(-\frac{2[(t - t_d)/\tau - b_1 z]^2}{f^2 - 8ib_2 z}\right), \end{aligned} \quad (13b)$$

$$\begin{aligned} \Omega_{p1-}^* &= \Omega_{p1}^*(0, 0) e^{ic_0 z} \frac{|\Omega_{c1}|^2}{|\Omega|^2 \sqrt{1 - 8ic_2 z}} \exp\left(-\frac{2(t_r/\tau - c_1 z)^2}{1 - 8ic_2 z}\right) \\ &\quad + \Omega_{p2}^*(0, t_d/\tau) e^{ic_0 z} \frac{\Omega_{c2}^* \Omega_{c1}}{|\Omega\tau|^2 \sqrt{1 - 8ic_2 z/f^2}} \\ &\quad \times \exp\left(-\frac{2[(t - t_d)/\tau - c_1 z]^2}{f^2 - 8ic_2 z}\right). \end{aligned} \quad (13c)$$

Equations (13a)–(13c) indicate that *nonadiabatic corrections contribute to both pulse spreading and attenuation*. The pulse breakup cannot be avoided because of the pulse delay and the difference in pulse lengths. The Ω_{p1+}^* component, however, can be significantly reduced by properly choosing parameters that yield a large $\text{Im}[b_0]$, leaving two pulses [i.e., Ω_{p1-}^* components in Eq. (13c)] of different widths, separated by a delay of t_d , traveling at the *same* group velocity. An

expression for Ω_{p2}^* can be obtained similarly.

IV. COMPARISON WITH NUMERICAL CALCULATIONS

In this section we demonstrate the validity of the above-described analytical solutions by numerical calculations of the inverse transform of Eq. (3). Examples shown in this section are appropriate to ultracold ^{87}Rb atomic vapors where Doppler broadening is negligible. Typical densities of such ultracold and Bose-Einstein-condensed atomic vapors range from a few times 10^{13} cm^{-3} to a few times 10^{14} cm^{-3} [20,21]. With these experimentally achievable parameters, we now demonstrate that it is possible to observe the high efficiencies discussed in the present study.

Let us choose $|1\rangle=5S_{1/2}(F=1, M_F=-1)$, $|2\rangle=5P_{1/2}(F=2, M_F=0)$, and $|3\rangle=5S_{1/2}(F=2, M_F=1)$. The splitting between the $5P_{1/2}(F=1)$ and $5P_{1/2}(F=2)$ levels is 816 MHz, so we choose $\delta_{p2}=1.256 \times 10^9\text{ s}^{-1}$ (≈ 200 MHz) and $\delta_{p1}=0$ for group velocity matching. Since the lifetime of the $5P_{1/2}$ level is $27.7 \times 10^{-9}\text{ s}$, we have $\gamma_2=3.61 \times 10^7\text{ s}^{-1}$. We consider co-propagating beams with the probe and control lasers having σ_+ and σ_- polarizations, respectively. Taking $D_{12}=2.20 \times 10^{-18}\text{ esu cm}$, $D_{23}=3.81 \times 10^{-18}\text{ esu cm}$, and $N=10^{14}\text{ cm}^{-3}$, we have $\kappa_{12}=2.28 \times 10^{11}\text{ cm s}^{-1}$. If we choose a matched group velocity of $V_g=40\text{ m/s}$, we obtain $|\Omega_{cn}|=2.14 \times 10^7\text{ s}^{-1}$. Finally, we assume a Gaussian input pulse shape with a full width at $1/e$ of τ . In particular, we choose $\tau=10^{-4}\text{ s}$. We further assume that the decay rate of the coherence between states $|1\rangle$ and $|3\rangle$ is $\gamma_3=500\text{ s}^{-1}$. Thus the set of parameters used in the following numerical calculations is

$$|\Omega_{cn}\tau|=2136, \quad \gamma_2\tau=3610, \quad \kappa_{12}\tau=2.28 \times 10^7\text{ cm}^{-1},$$

$$\delta_{p2}\tau=1.256 \times 10^5, \quad \gamma_3\tau=0.05, \quad \delta_{p1}\tau=0,$$

$$V_g^{(-)}\tau=0.4\text{ cm}.$$

We first consider the case where $\Omega_{p1}(0,0)\tau=1$ and $\Omega_{p2}(0,0)\tau=0$. Here we are interested in demonstrating the possibility of high photon flux conversion efficiency from the ω_{p1} mode of probe laser to the FWM field (i.e., ω_{p2} mode). To find the propagation distance where the first destructive interference occurs we set [see Eqs. (8a) and (8b)] $2\kappa_{12}\tau z_1/(\delta_{p2}\tau)=\pi$ and find $z_1=0.00865\text{ cm}$. Thus we choose the maximum medium thickness to be $z_m=z_1=0.01\text{ cm}$. Using the parameters shown above, we plot, in Fig. 2, Eqs. (8a) and (8b) (solid and dashed lines) along with the numerical inverse transforms of Eq. (3) (dotted and dot-dashed lines). The results from Eqs. (8a) and (8b) are so close to the results from Eq. (3) that they cannot be distinguished on the graph. The difference in these results is less than 2% at all points except near the zeros of the functions. Note that the largest value for $|\Omega_{p2}(z, t_r/\tau)|^2/|\Omega_{p1}(0,0)|^2$ is near $z=0.0865\text{ cm}$, as predicted. This value is slightly larger than 0.91, implying a conversion efficiency of 91%. Most of the difference from 100% is due to the decay of the second term (e.g., the factor $\exp[-2\gamma_2\tau\kappa_{12}\tau z/(\delta_{p2}\tau)^2]$). Thus, at the peak, instead of having $(1/4)(2)^2=1$ at the point of construc-

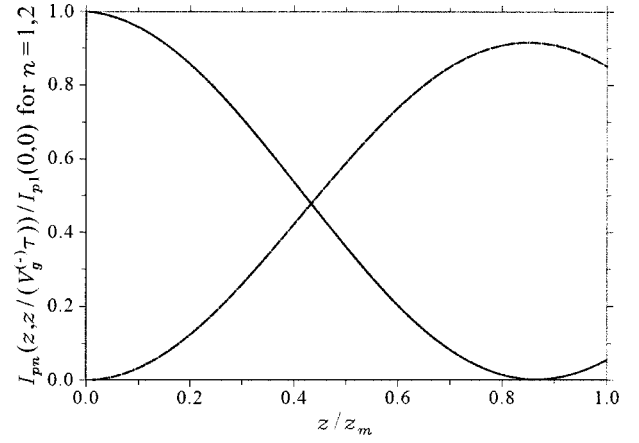


FIG. 2. Normalized peak intensity of the ω_{p1} mode (solid line) and ω_{p2} mode (dashed line) as a function of z/z_m for a given medium length. Parameters used: $|\Omega_{c1}\tau|=|\Omega_{c2}\tau|=2136$, $\delta_{p1}\tau=0$, $\delta_{p2}\tau=1.256 \times 10^5$, $|\Omega_{p1}(0,0)\tau|=1$, $|\Omega_{p2}(0,0)\tau|=0$, $\gamma_2\tau=3610$, $\delta_3\tau=0$, $\gamma_3\tau=0.05$, $f=1$, $t_d/\tau=0$, $\kappa_{12}\tau=2.28 \times 10^7\text{ (cm s)}^{-1}$, and $z_m=0.01\text{ cm}$. Each curve contains two curves: one obtained from Eq. (3) and the other obtained from Eqs. (8a) and (8b). The agreement between the two equations is excellent and the curves cannot be distinguished.

tive interference, we have $(1/4)[1+\exp(-0.0902)]^2=0.9156$. Note that if the concentration had been taken to be $N=5 \times 10^{14}\text{ cm}^{-3}$, then the constructive interference would have occurred at $z=0.0018\text{ cm}$, which is well within the range of parameters that have already been demonstrated in laboratories for ultracold atomic vapors.

In the second example we show how small the attenuation of the slowly decaying terms in Eqs. (3), (8a), and (8b) actually are after the one- and three-photon destructive interference has become effective. In Fig. 3 we replot Fig. 2 for $z_m=1\text{ cm}$, even though currently there is no ultracold system that can reach this length yet still have a density of $N \approx 10^{14}\text{ cm}^{-3}$. This figure shows that after almost 300 times

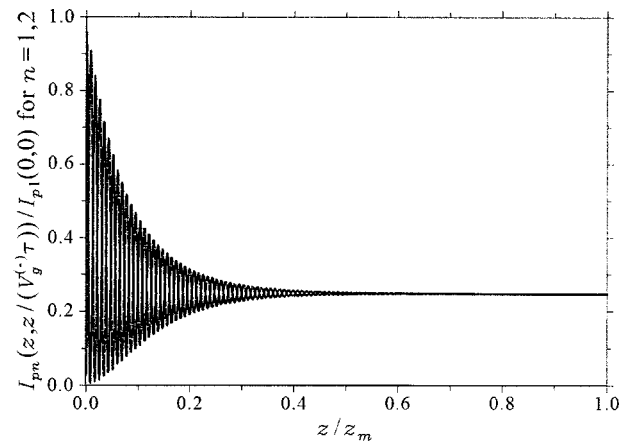


FIG. 3. Same as Fig. 2 except $z_m=1.0\text{ cm}$. As in Fig. 2, the agreement between solutions obtained from Eqs. (3), (8a), and (8b) is excellent and the curves cannot be distinguished. Although the large propagation depths are not available experimentally, this figure demonstrates just how transparent the medium is over such great depths when Eq. (10) is satisfied.

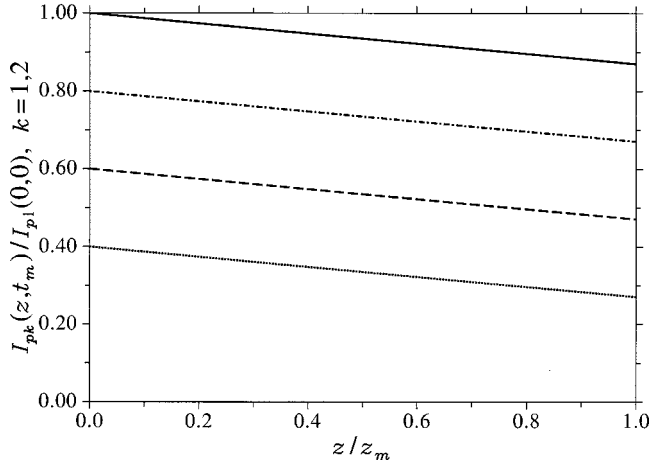


FIG. 4. Same as Fig. 3 except $|\Omega_{p2}(0,0)\tau|=1$. In this case, a highly efficient multiphoton destructive interference creates an induced transparency that renders the medium highly transparent when the intensity of the two modes satisfies Eq. (10). There are four curves in the figure with two for each mode (solid line and dash-dotted lines for ω_{p1} , dashed line, and dotted line for ω_{p2}) using Eqs. (3), (8a), and (8b). The lower three curves are results of adding 0.2, 0.4, and 0.6 offsets, respectively, for better viewing. Without these offsets, the four curves cannot be distinguished, indicating the excellent agreement between Eqs. (3), (8a), and (8b).

the propagation distance (in comparison with Fig. 2) the amplitudes of the slowly decaying part of Eqs. (3), (8a), and (8b) have only decayed by a factor of $\exp[-\gamma_3 z_m / (2V_g^{(-)})] \simeq e^{-0.0625} = 0.94$ from 0.25 which is the maximum (i.e., 100%) photon flux conversion efficiency for the initial condition $\Omega_{p2}(0,0)=0$. Again, as shown in Fig. 3, the approximate solutions Eqs. (8a) and (8b) agree well with the numerical evaluation of Eq. (3).

We now demonstrate what one should expect when Eq. (10) is satisfied. We start with the case where all parameters are the same as in Fig. 3, except $\Omega_{p1}(0,0)\tau = \Omega_{p2}(0,0)\tau = 1$. In this case we expect that the medium will be transparent to both fields for the entire $z_m = 1$ cm propagation distance even at a concentration of 10^{14} cm $^{-3}$. Thus, except for the factor of $\exp[-\gamma_3 z_m / (2V_g^{(-)})]$, we expect the amplitudes of both modes to remain near unity. Figure 4 again shows the results from Eqs. (3), (8a), and (8b) for both modes. In this figure we have four curves that cannot be distinguished, demonstrating the agreement between the analytical solutions [Eqs. (8a) and (8b)] and the numerical evaluation of Eq. (3).

We now present numerical calculations using Eqs. (11) and (13a)–(13c). To be specific, we take the field profiles, Eq. (12) and compare analytical solutions based on the quadratic approximation, Eqs. (11) and (13a)–(13c), and the numerical solution by directly integrating using Eqs. (1a)–(1d). The parameters used here are different from those used in the linear approximations. Here we have purposely chosen the parameters such that the adiabatic approximations are not very robust to demonstrate yet still very good agreement between the analytical treatment and rigorous numerical calculations. We first take $|\Omega_{c1}\tau| = |\Omega_{c2}\tau| = 50$, $\delta_{p1}\tau = 200$, $\delta_{p2}\tau = 250$, $|\Omega_{p1}(0,0)\tau| = 1$, $|\Omega_{p2}(0,0)\tau| = 1/2$, and $\gamma_2\tau = 10$, with $f=1$ and $t_d/\tau=0$. In Fig. 5, we have plotted the normalized

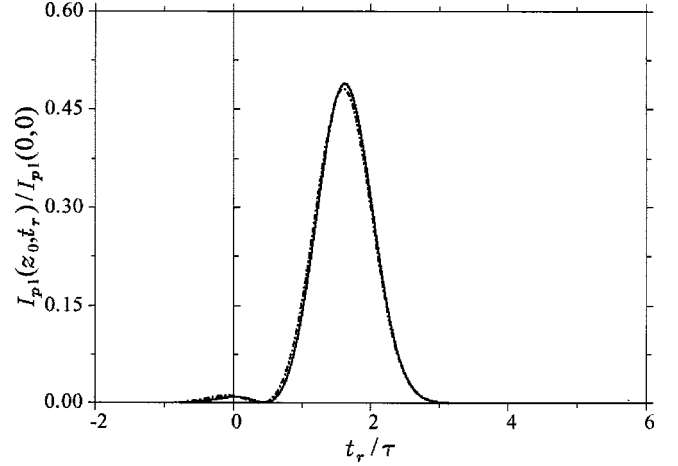


FIG. 5. Normalized intensity of the ω_{p1} mode probe wave as a function of t_r/τ for a given medium length. The calculation is based on quadratic approximations Eqs. (11) and (13a)–(13c) for the field profiles, Eq. (12), and parameters are chosen for less robust adiabatic process. Parameters used: $|\Omega_{c1}\tau| = |\Omega_{c2}\tau| = 50$, $\delta_{p1}\tau = 200$, $\delta_{p2}\tau = 250$, $|\Omega_{p1}(0,0)\tau| = 1$, $|\Omega_{p2}(0,0)\tau| = 1/2$, $\gamma_2\tau = 10$, $\delta_3\tau = 0$, $\gamma_3\tau = 0.01$, $f=1$, $t_d/\tau=0$, and $\kappa_{12}\tau z = 8000$. Solid curve: numerical evaluation of Eqs. (1a)–(1d). Dashed curve: analytical results based on the quadratic approximation of Eq. (13a)–(13c). The analytical treatment predicts a large peak (Ω_{p1-}) at $t_r/\tau = 1.6$ (corresponding to a group velocity of 1.6×10^3 m/s for $\tau = 10^{-5}$ s and $z = 1$ cm) and a small peak (Ω_{p1+}) at $t_r/\tau = 0.01$. We have intentionally chosen the parameters so that the Ω_{p1+} part of the wave is still visible.

probe intensity (mode ω_{p1}) as a function of t_r/τ for a given medium length. The solid curve is obtained by direct numerical integration of Eqs. (1a)–(1d), and the dashed curve was obtained using the analytical expression resulting from the quadratic approximation, Eqs. (11) and (13a)–(13c). The latter predicts a large peak (Ω_{p1-}) at $t_r/\tau = 1.6$, corresponding to a group velocity of 10^3 m/s, and a small peak (Ω_{p1+}) at $t_r/\tau = 0.01$. The excellent agreement between these two methods indicates the validity of the quadratic approximation under the conditions specified.

Finally, we consider the case where $\Omega_{p1}(0,0)\tau = 1$ and $\Omega_{p2}(0,0)\tau = 0$ in the quadratic approximation. As have been discussed before, this single-probe two-control configuration converts the photons from the Ω_{p1} field to the Ω_{p2} field via a FWM process. With the detuning δ_{p1} fixed, changing the detuning δ_{p2} results in a tunable FWM field (Ω_{p2}) with a high photon flux conversion efficiency. This is a potentially very useful narrow-band tunable coherent source. Taking the parameters given in Fig. 6 our analytical treatment predicts a large peak (Ω_{p1-}) at $t_r/\tau = 1.6$, corresponding to a group velocity of 1.6×10^3 m/s (for $\tau = 10^{-5}$ s and $z = 1$ cm), and a small peak (Ω_{p1+}) at $t_r/\tau = 0.01$. This can be seen in Fig. 3 where the normalized intensity of the FWM field as a function of t_r/τ is plotted. We have chosen the parameters such that the fast wave has nearly zero amplitude. It is seen that the numerical results agree well with the above theoretical prediction. Further numerical calculations have shown that under the conditions specified, the results are in very good agreement with the analytical solutions of Eq. (13a)–(13c). In fact, typical errors between these methods are $< 2\%$.

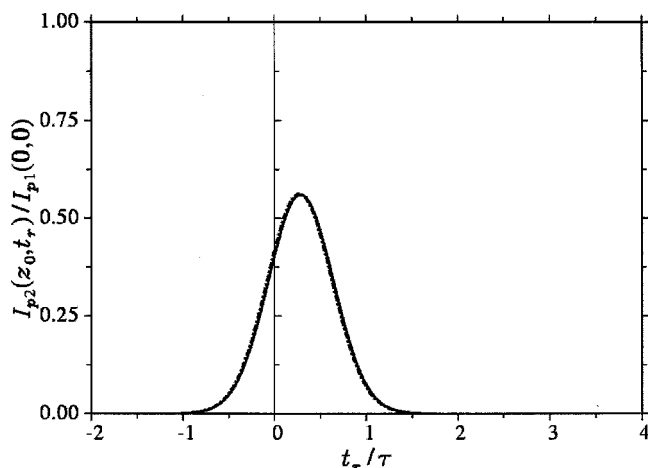


FIG. 6. Normalized intensity of the FWM field (Ω_{p2}) as a function of t_r/τ for a given medium length. Parameters: $|\Omega_{p1}(0,0)\tau|=1$, $|\Omega_{p2}(0,0)\tau|=0$, $\delta_{p1}\tau=0$, $\delta_{p2}\tau=1250$, $\gamma_2\tau=25$, $\delta_3\tau=0$, $\gamma_3\tau=0.01$, $|\Omega_{c1}\tau|=|\Omega_{c2}\tau|=200$, $f=1$, $t_d/\tau=0$, and $\kappa_{12}\tau z=19\,625$. The solid curve is from the numerical integration of Eqs. (1a)–(1d). The dashed curve is obtained from Eq. (13a)–(13c). The parameters are chosen so that the Ω_{p1+}^* part of the wave dampens out completely.

V. SUMMARY

We have proposed a two-mode, single-specie three-level Λ system to achieve TAG matched pairs of ultraslow waves and have shown a type of induced transparency process that is established by a multiphoton destructive interference. In the linear and quadratic approximation, we have shown that after a characteristic propagation distance both probe modes

evolve into a TAG matched pulse pair which travels without distortion and attenuation in a highly dispersive medium with an atomic density as high as 10^{14} cm^{-3} . This is a remarkably efficient transparency scheme, and we have demonstrated nearly 100% photon flux conversion efficiency from one mode to another. In addition, we have shown that the proposed scheme does not require maximum atomic coherence. Indeed, there is very little atomic coherence ($\ll 0.5$) in the system we studied. This is to be contrasted to other schemes where maximum atomic coherence is required [4].

We have also compared our linear and quadratic approximations with numerical calculations for several examples using experimental achievable parameters. These comparisons have shown that the analytic solutions agree well with numerical calculations under the conditions specified.

Generation of TAG matched ultraslow waves using a single-specie three-level medium may have important applications. The concept applies to multiwavelength schemes and is readily scalable to single-photon regimes. This may open possibilities of quantum entanglement of ultraslow photon pairs and quantum computation using ultraslow optical fields. The FWM characteristics of the two-mode ultraslow-wave scheme also opens the possibility of multiple-wave mixing in ultraslow propagation regimes. With a single probe field Ω_{p1} as the input, adjusting δ_{p2} will generate a tunable FWM field Ω_{p2} with near 100% photon flux conversion efficiency.

ACKNOWLEDGMENT

This research is supported in part by the Office of Naval Research under Contract No. N001403IP20106.

- [1] O. A. Kocharovskaya and Y. I. Khanin, *JETP Lett.* **48**, 630 (1988); K. J. Boller, A. Imamoglu, and S. E. Harris, *Phys. Rev. Lett.* **66**, 2593 (1991); S. E. Harris, *Phys. Today* **50**(7), 36 (1997).
- [2] G. Alber *et al.*, *Quantum Information* (Springer-Verlag, Berlin, 2001).
- [3] O. Schmidt, R. Wynands, Z. Hussein, and D. Meschede, *Phys. Rev. A* **53**, R27 (1996); G. Müller, A. Wicht, R. Rinkleff, and K. Danzmann, *Opt. Commun.* **127**, 37 (1996); A. M. Akulshin, S. Barreiro, and A. Lezama, *Phys. Rev. Lett.* **83**, 4277 (1999); M. M. Kash *et al.*, *ibid.* **82**, 5229 (1999); L. V. Hau *et al.*, *Nature (London)* **397**, 594 (1999).
- [4] M. Jain *et al.*, *Phys. Rev. Lett.* **77**, 4326 (1996); A. J. Merriam *et al.*, *ibid.* **84**, 5308 (2000); M. D. Lukin, *Adv. At., Mol., Opt. Phys.* **42**, 347 (2000).
- [5] Liwei Wang *et al.*, *Phys. Rev. A* **46**, 7192 (1992); C. W. Law and J. H. Eberly, *ibid.* **47**, 3195 (1993); Liwei Wang and J. H. Eberly, *ibid.* **47**, 4248 (1993).
- [6] H. Schmidt and R. J. Ram, *Appl. Phys. Lett.* **76**, 3173 (2000); A. F. Huss *et al.*, *Phys. Rev. A* **63**, 013802 (2000); B. S. Ham and P. R. Hemmer, *Phys. Rev. B* **68**, 073102 (2003).
- [7] M. D. Lukin and A. Imamoglu, *Phys. Rev. Lett.* **84**, 1419 (2000).
- [8] D. Petrosyan and G. Kurizki, *Phys. Rev. A* **65**, 033833 (2002).
- [9] D. Budker, D. F. Kimball, S. M. Rochester, and V. V. Yashchuk, *Phys. Rev. Lett.* **83**, 1767 (1999).
- [10] S. E. Harris and L. Hau, *Phys. Rev. Lett.* **82**, 4611 (1999).
- [11] C. Ottaviani *et al.*, *Phys. Rev. Lett.* **90**, 197902 (2003).
- [12] L. Deng *et al.*, *Phys. Rev. Lett.* **88**, 143902 (2002).
- [13] M. G. Payne and L. Deng, *Phys. Rev. A* **65**, 063806 (2002).
- [14] M. G. Payne and L. Deng, *Phys. Rev. Lett.* **91**, 123602 (2003).
- [15] For early works on bichromatically driven two-level systems see Z. Ficek and H. S. Freedhoff, *Phys. Rev. A* **53**, 4275 (1996) and references therein.
- [16] Dual ultraslow waves have been proposed in [7,8] in the context of Kerr nonlinearity. The former relies on two multistate species whereas the latter requires a single-specie medium of six states.
- [17] For temporally matched strong pulses see S. E. Harris, *Phys. Rev. Lett.* **70**, 552 (1992); **72**, 52 (1994).
- [18] J. C. Miller *et al.*, *Phys. Rev. Lett.* **45**, 114 (1980); D. J. Jackson and J. J. Wynne, *ibid.* **49**, 543 (1982); M. G. Payne and W. R. Garrett, *Phys. Rev. A* **28**, 3409 (1983); M. G. Payne, W. R. Ferrell, and W. R. Garrett, *ibid.* **27**, 3053 (1983); M. G. Payne *et al.*, *ibid.* **44**, 7684 (1991); R. K. Wunderlich *et al.*, *ibid.* **41**, 6345 (1990); L. Deng *et al.*, *Phys. Rev. Lett.* **73**,

2035 (1994).

- [19] Although high conversion efficiency can be achieved with ultraslow group velocities, it can also be achieved with fast waves depending on the conditions. In the optically thin medium, the fast-wave scheme can achieve a better conversion efficiency than the slow-wave scheme. In the optically thick medium, however, the slow-wave scheme may offer a much better conversion efficiency in some nonlinear processes depending on the excitation schemes.
- [20] The decay rates used in the Schrödinger picture are, in general,

a combination of population and coherence decay rates used in density matrix formalism. The conditions used in the present study ensure the equivalence between Schrödinger wave function formalism and more rigorous density matrix formalism. By constructing density matrix elements using Schrödinger wave function, one obtains the relations between decay rates in two different formalisms.

- [21] Such as the Bose condensate with $N \approx 5 \times 10^{14} \text{ cm}^{-3}$ at MIT and $N \approx 5 \times 10^{13} \text{ cm}^{-3}$ at NIST Gaithersburg.